

## Original article

# Preparation and investigation of self-healing gel for mitigating circulation loss

Ren Wang<sup>1</sup>, Cheng Wang<sup>1,2</sup>, Yifu Long<sup>1</sup>, Jinsheng Sun<sup>1</sup>\*, Luman Liu<sup>1</sup>, Jianlong Wang<sup>1</sup>

<sup>1</sup>CNPC Engineering Technology R&D Company Limited, Beijing 102206, P. R. China

<sup>2</sup>College of Chemistry and Chemical Engineering, Southwest Petroleum University, Chengdu 610500, P. R. China

### Keywords:

Self-healing  
lost circulation materials  
drilling fluid  
curdlan

### Cited as:

Wang, R., Wang, C., Long, Y., Sun, J., Liu, L., Wang, J. Preparation and investigation of self-healing gel for mitigating circulation loss. *Advances in Geo-Energy Research*, 2023, 8(2): 112-125.  
<https://doi.org/10.46690/ager.2023.05.05>

### Abstract:

Lost circulation is a common and complex downhole accident in the process of oil and gas drilling. Traditional bridge plugging material has the limitation of poor adaptability to lost formations. Therefore, this study synthesized a new self-healing plugging material to improve the plugging success rate; specifically, the hydrophobic association polymer lauryl methacrylate-acrylamide-acrylic acid containing  $\text{Fe}^{3+}$  was modified via curdlan to form a composite gel with high strength and self-healing properties. The self-healing time, mechanicalness and rheological properties of the self-healing gel were systematically evaluated. The results showed that the modification of curdlan could significantly improve the mechanical properties and rheological strength of self-healing gel, and the chelating structure formed by  $\text{Fe}^{3+}$  and carboxyl groups could further enhance the mechanical properties of the self-healing gel. Toughness and storage modulus of the  $\text{LF}_{0.15}\text{C}_2$  self-healing gel with the introduction of curdlan and  $\text{Fe}^{3+}$  could reach  $30.2 \text{ kJ/m}^3$  and  $3,458 \text{ Pa}$ , respectively. Compared with conventional gel materials, composite gels with self-healing properties exhibited better pressure-bearing capacity of  $2.5 \text{ MPa}$ , and could effectively avoid causing plugging at the entrance of the fractures by high-concentration inert material and improve the pressure-bearing capacity. In addition, the plugging mechanism of the self-healing gel modified via curdlan in formation fractures was analysed in detail. The self-healing gel modified via curdlan prepared in this work has application potential as a lost circulation material in the field of oil and gas drilling.

## 1. Introduction

Lost circulation refers to the phenomenon in which well-bore working fluid leaks into the formation due to the differential pressure during downhole operations, such as oil and gas drilling, cementing, and testing (Abbas et al., 2019; Alkinani et al., 2019). Lost circulation is a popular and difficult problem in the field of oil and gas engineering. It not only consumes a large amount of working fluid loss but also directly causes major economic losses. Lost circulation also increases nonproduction time, prolongs drilling cycle, affects the exploration and development process, and even induces accidents, such as sticking, well collapse and blowout (Mansour et al., 2019; Zhao et al., 2019; Tang et al., 2022). Due to the complex problem of lost circulation, a commonly

used method is bridging plugging method; in the method, a certain amount of bridging plugging material is added to the drilling fluid according to the construction situation, and as the drilling fluid enters the lost circulation formation, the plugging layer is formed by filling and stacking to reduce the leakage rate and achieve plugging (Alhaidari et al., 2022). However, this method has the disadvantages of weak interaction between inert material interfaces and poor matching with fractures. Therefore, inorganic plugging materials, polymer plugging materials and other plugging materials have also extensively been studied (Pandya and Naik, 2016; Lian et al., 2018). Among them, gel material is a typical polymer plugging material, has been developed due to its excellent deformability and compactness, and is widely used in the field of petroleum engineering (Al-Ibadi and Civan, 2013; Ahdaya et al., 2022).

Self-healing gels is a gel system formed by reversible dynamic bond links such as ionic bonds, hydrogen bonds, hydrophobic association, and DA reactions (Feldner et al., 2016; Wang et al., 2023). The self-healing gel can spontaneously heal after being destroyed to complete the recovery of structure and function (Taylor and Panhuis, 2016; Christopher et al., 2020). Due to its unique self-healing properties, self-healing gels has been widely studied and applied in many fields in recent years, and their application in the field of conformance control and water shutoff agents has also been gradually carried out (Schuman et al., 2022). Thermo-elastic and self-healing polyacrylamide-2D nanofiller composite hydrogels was applied to water shutoff treatment (Michael et al., 2020). The particle gels with recrosslinking properties have been used to treat the problem of void space conduits and repair the "short-circuited" waterflood in Alaska's West Sak field (Zhao et al., 2023). However, there are few reports on the self-healing gels as lost circulation material (LCM), and the stability of self-healing gels during the formation is still a major challenge (Bai et al., 2022). Due to the considerable heterogeneity of the traditional self-healing gel structure, single crosslinking mode and lack of an effective energy dissipation mechanism, its mechanical properties are poor (Hussain et al., 2018).

Hydrophobic association is a reversible physical action that is usually formed by hydrophobic monomers and surfactants through hydrophobic lipophilic interactions (Tuncaboylu et al., 2011). As a network cross-linking point, the hydrophobic association microregion has a dynamic association-disassociation balance, provides good self-healing performance of the gel. Moreover, due to the strong binding energy of the hydrophobic association and the stability in a water environment, the hydrophobic part of the polymer chain can be removed from the free radical micelle to dissipate energy (Davydovich and Urban, 2020). Curdlan is a linear macromolecular polysaccharide linked by  $\beta$ -1,3-linked glucose bonds. The most special property of curdlan is its ability to be heated into gel (Aquinas et al., 2022). When curdlan is heated to 55~80 °C, curdlan will form a thermally reversible gel. When the heating temperature is higher than 80 °C, the gel formed by curdlan is a thermally irreversible gel, and the gel will not dissolve after heating to 120 °C (Hino et al., 2003). At present, there are few reports on lost circulation control using curdlan. Therefore, modification of hydrophobically associating polymers by curdlan has important research significance.

In this work, lauryl methacrylate (LMA) was used as a hydrophobic monomer, acrylamide (AM) and acrylic acid (AA) were used as hydrophilic monomers to form a hydrophobic association polymer LMA-AM-AA with self-healing properties. Then  $\text{Fe}^{3+}$  and curdlan were introduced to form a composite gel with the polymer LMA-AM-AA, and the mechanical strength was improved. The physical and chemical properties of the self-healing gel were studied via Fourier transform infrared spectroscopy (FT-IR), scanning electron microscope (SEM) and thermogravimetric analysis (TGA). The self-healing time, mechanical properties and rheological properties of the self-healing gel were systematically studied. The effects of reaction temperature, pressure and time on the rheological strength of the self-healing gel were investigated.

**Table 1.** Components for the preparation of the different samples.

Samples	$\text{FeCl}_3 \cdot 6\text{H}_2\text{O}$ (g)	Curdlan (g)
LF <sub>0</sub> C <sub>0</sub>	0	0
LF <sub>0.15</sub> C <sub>0</sub>	0.15	0
LF <sub>0</sub> C <sub>2</sub>	0	2
LF <sub>0.15</sub> C <sub>2</sub>	0.15	2
LF <sub>0.05</sub> C <sub>2</sub>	0.05	2
LF <sub>0.25</sub> C <sub>2</sub>	0.25	2
LF <sub>0.15</sub> C <sub>1</sub>	0.15	1
LF <sub>0.15</sub> C <sub>3</sub>	0.15	3

The plugging performance of the self-healing gel was also investigated.

## 2. Materials and methods

### 2.1 Materials

Acrylamide (AM, 99%), acrylic acid (AA, 98%), lauryl methacrylate (LMA, 99%), sodium dodecyl sulfate (SDS, 99%), N, N-methylenbisacrylamide bis-acrylamide (MBA, 99%), sodium chloride (NaCl, 99.5%), calcium chloride anhydrous ( $\text{CaCl}_2$ , 96%), ferric chloride hexahydrate ( $\text{FeCl}_3 \cdot 6\text{H}_2\text{O}$ , 99%) and ammonium persulphate (APS, 99%) were obtained from McLean Technology Co., Ltd, Shanghai, China. Curdlan was purchased from Shandong Zhongke Biotechnology Co. Ltd, Shandong, China.

### 2.2 Preparation of self-healing gels

First, 0.15 g  $\text{FeCl}_3 \cdot 6\text{H}_2\text{O}$  was added to a 0.5 mol/L NaCl solution. Then 7 g SDS was added and dissolved at 35 °C for 2 h. Next, 0.8 g LMA was added to the above solution and stirred at 35 °C for 4 h. After, 17 g AM and 6.5 g AA were added and stirred for 1 h. Different amounts of curdlan were slowly added to the above solution and stirred at room temperature for 30 h. Finally, 0.2 g APS was added, stirred and used to dissolve the obtained dispersion in a 45 °C water bath for 4 h; the mixture was then placed in a 90 °C water bath for 30 min to obtain the curdlan-modified self-healing gel. To investigate the effects of different components, samples with different formulations were prepared (Table 1), and the amounts of LMA, AM and AA in all samples were 0.8, 17 and 6.5 g, respectively. In contrast, conventional gels (PAM) without self-healing properties were prepared by using monomers (AM, AA) and 0.1% (wt% to total monomer) of MBA. All prepared gels were cut into small pieces, and then dried in vacuum at 50 °C for 30 h. Finally, the prepared samples were crushed into gel particles with a particle size of 1-3 mm.

### 2.3 Characterizations

The functional groups in the self-healing gels were determined by Fourier transform infrared spectroscopy (FT-IR, WQF520, Beijing, China) with the assistance of KBr in a wavenumber range of 4,000~800  $\text{cm}^{-1}$ . Morphology of self-

healing gels were characterized using a scanning electron microscope (SEM, ZEISS EVO18, Oberkochen, Germany) at 5 and 15 kV acceleration voltage, and all the samples were freeze-dried and coated with Au before the measurement. Thermal stability of self-healing gel was measured through thermogravimetric analysis (TGA, NetzschSTA449F3, Selb, Germany) in a nitrogen atmosphere with a heating rate of 10 °C/min that changed from ambient temperature to 500 °C.

#### 2.4 Self-healing time and swelling behaviour measurements

Self-healing time of the samples were determined via the bottle test method. The self-healing gel particles were added to 5% bentonite to prepare a dispersion with a gel particle concentration of 10%. After stirring, they were placed in an oven at 90 °C. The morphology of the sample was examined every 0.5 hour. The self-healing time was divided into the self-healing start time and end time. The self-healing start time was the time when a weak correlation occurred between the gels, and the end time was the time when the boundary between the gels disappeared and became a whole gel. In our study, the self-healing time was defined as the time from when the sample was placed in the oven to the end of the self-healing process.

Swelling behaviour of gel particles in bentonite mud was measured. Specifically, the gel particles with initial mass  $M_0$  were placed in an excess of 5% bentonite mud and swelled at different temperatures. The mass  $M_t$  of the gel was recorded at intervals, and the swelling ratio ( $R$ ) of the sample was determined:

$$R = \frac{M_t - M_0}{M_0} \quad (1)$$

where  $M_0$  and  $M_t$  are the mass of the sample at the initial time and time  $t$ , respectively.

#### 2.5 Mechanical and rheological tests

Mechanical (tensile and compressive properties) tests of self-healing gel were performed by a universal electromechanical tester (WH-50, Weiheng, China). For the uniaxial tensile test sample, the sample was cut into a rectangular shape with a length of 50 mm, a width of 15 mm, and a thickness of 5 mm; a tensile rate of 60 mm/min and the distance between the two fixtures of 25 mm were used for this test. For the compression test sample, the sample was prepared into a cylinder with a diameter of 10 mm and a height of 15 mm; a compression rate of 5 mm/min and compression to 90% compression strain were used for this test.

The rheological test of the self-healing gel was carried out by a rotary rheometer (MCR 320e, Anton Paar, Austria) with a plate spacing of 1 mm. A fixed frequency of strain scanning was 6.28 rad/s, and the strain amplitude scanning range was 0.1%~1000%. The viscoelastic range of the self-healing gel was determined by the strain scanning. In the viscoelastic range of the sample, the strain was fixed at 1% and the frequency scanning was carried out in the frequency range of 0.1~100 rad/s. Finally, the curves of storage modulus  $G'$

and loss modulus  $G''$  with strain and frequency were obtained. The value of  $G'$  was the average value of  $G'$  in the viscoelastic interval.

#### 2.6 Effect of reaction time, pressure and temperature on self-healing gel properties

Effect of reaction time, pressure and temperature on self-healing gel properties were investigated by a temperature–pressure reaction device (Figs. S1 and S2). The self-healing gel particles were added to 5% bentonite mud to prepare a dispersion with a gel particle concentration of 10%, and then the dispersion was placed in the reactor. After it was completely absorbed, the pressure was injected into the reactor through the hydraulic pump and the reaction temperature was set. After the reaction, the gel was removed from the reactor, and the rheological properties of the self-healing gel were tested via rheometer.

#### 2.7 Plugging performance tests

The plugging performance of the self-healing gel was evaluated. Through the plugging evaluation device (Figs. 1 and S3), the sample particles were initially mixed with 5% bentonite mud to prepare a plugging slurry with a self-healing gel particle concentration of 10%. Then the plugging slurry was injected into the fractured metal core (length of 150 mm, inlet and outlet fracture widths of 3 mm and 1 mm, respectively) at a speed of 5 mL/min with an advection pump. Next, the fractured metal core was placed in an ageing tank containing 20 mL bentonite mud and kept at 90 °C for 12 h. After, the fractured metal core was placed in the holder, the liquid outlet valve was opened, and 2 L bentonite mud was injected into the container. The displacement pressure was set to 0.5 MPa, and 0.5 MPa was increased every 2 min until the liquid continuously flowed out from the outlet. When the shell is used as LCM, the initial pressure and pressure gradient are both 1 MPa. At this time, the maximum pressure was the pressure bearing capacity of the sample.

### 3. Results and discussion

#### 3.1 Synthesis of the self-healing gel

The self-healing gel modified by curdlan was prepared by a simple method, and the synthesis scheme is shown in Fig. 2. Initially, under the action of heating and an initiator, the solubilized hydrophobic monomer (LMA) in the SDS micelle was copolymerized with the hydrophilic monomer (AM, AA) via free radical addition polymerization to form the LMA-AM-AA polymer, and the solubilized SMA in the SDS micelle was polymerized to form P(LMA) as a hydrophobic association crosslinking point (Qin et al., 2018). The carboxyl group on the polymer chain formed a coordination chelating structure with  $\text{Fe}^{3+}$ . Then, under further heating, the internal molecular chain of curdlan was transformed into a six-fold triple helix structure, and the gel was further formed via the hydrophobic interaction between the methyl groups of d-glycosyl residue C-6 on different molecular chains (Hino et al., 2003; Ye et al., 2020).

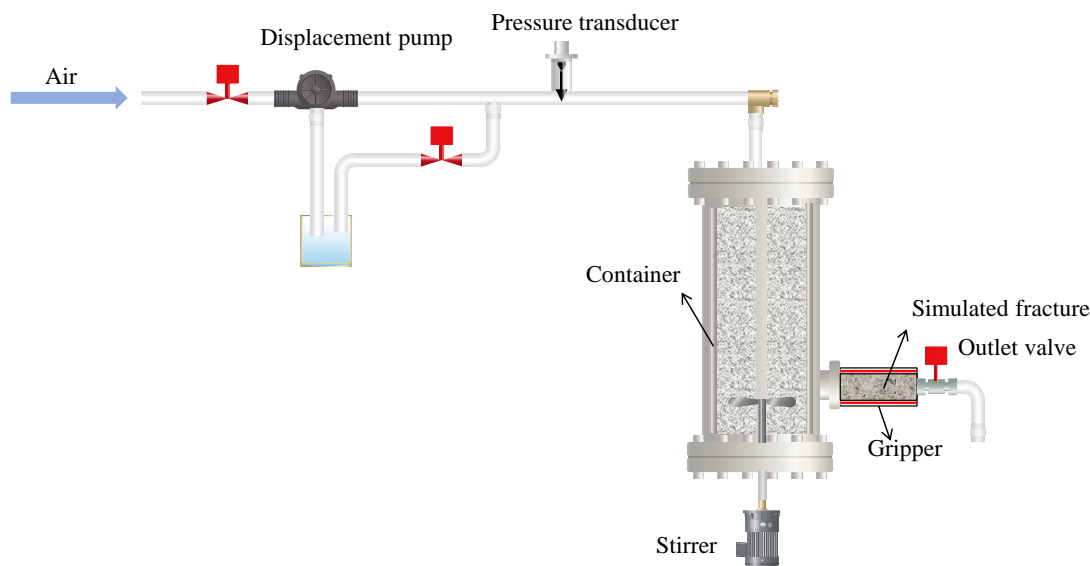


Fig. 1. Schematic diagram of the plugging performance test experiment.

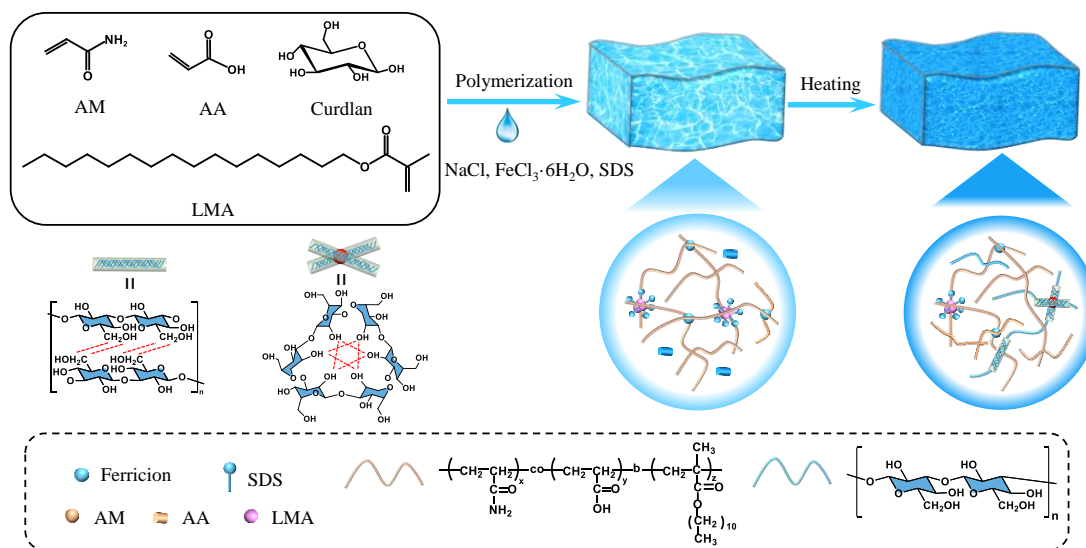


Fig. 2. Schematic illustration of the synthesis for self-healing gel.

### 3.2 Characterizations of the self-healing gel

To determine the functional groups in the self-healing gel, different samples were characterized via FT-IR, and the results are shown in Fig. 3(a). The wide absorption peak near 3,428 cm<sup>-1</sup> corresponded to the stretching vibration of -OH. The absorption peaks near 2,930 cm<sup>-1</sup> and 2,853 cm<sup>-1</sup> were caused by the stretching vibration of C-H group on LMA (Zeng et al., 2022). The characteristic peaks near 1,650 cm<sup>-1</sup> and 1,457 cm<sup>-1</sup> corresponded to the stretching vibration of -COO- on AA (Qin et al., 2018). This indicated that the copolymers of AA, AM and LMA were successfully synthesized. The characteristic peaks of the  $\beta$ -1,3-glycosidic bond in curdlan were detected near 1,175 cm<sup>-1</sup> and 887 cm<sup>-1</sup>, indicating that the copolymer and curdlan were successfully formed into composite gel (Hsieh et al., 2017). By comparing the FT-IR spectra of the samples before and after the introduction

of Fe<sup>3+</sup>, no new absorption peaks were observed after the introduction of Fe<sup>3+</sup>, which indicates that the introduction of Fe<sup>3+</sup> did not change the main functional groups of the molecule (Qin et al., 2018).

Thermal stability is a key indicator of LCM, and the weight loss curves of different samples under nitrogen were analysed. From Fig. 3(b), the TGA curves of all samples showed the same weight loss trend, and the weight loss below 207 °C was predominantly caused by the evaporation of bound water and free water in the sample. The weight loss stage at approximately 207~345 °C was mainly due to the decomposition of the carboxyl group in the molecular chain of the gel particle, the release in the form of CO<sub>2</sub>, and the formation of an imine structure or the formation of dehydrated ammonia released from the adjacent two amino groups on the side chain (Zheng et al., 2020). The weight loss after 345

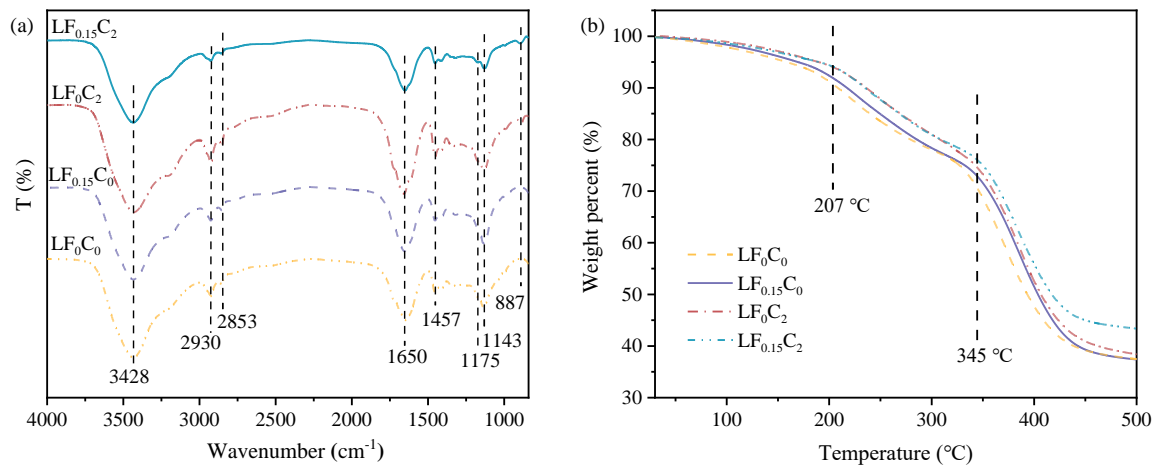


**Fig. 3.** Characterization results of the different samples. (a) FT-IR spectra of the different samples and (b) TGA curves of the different samples.

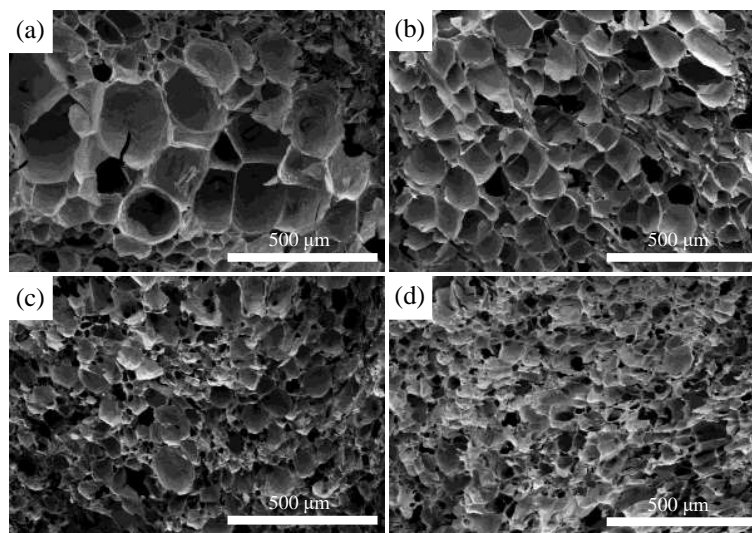


**Fig. 4.** SEM images of different samples. (a)  $LF_0C_0$ , (b)  $LF_{0.15}C_0$ , (c)  $LF_0C_2$  and (d)  $LF_{0.15}C_2$ .

°C corresponded to the further decomposition of curdlan and the decomposition of LMA-AM-AA macromolecular skeleton (Marubayashi et al., 2014). Clearly, the  $LF_{0.15}C_2$  sample with the introduction of curdlan and  $Fe^{3+}$  had a higher stability and greater residual mass.

To explore the microstructure of the self-healing gels, the self-healing gels were characterized by SEM after freeze-drying (Fig. 4).  $LF_0C_0$  sample and  $LF_{0.15}C_0$  sample showed evident uniform porous structures. However, the pore size of  $LF_{0.15}C_0$  sample was more compact, which was caused by the formation of a coordination structure with the carboxyl groups in the molecular chain after the introduction of  $Fe^{3+}$  (Zheng et al., 2020). Compared with  $LF_0C_0$  and  $LF_{0.15}C_0$ , the three-dimensional network structure of  $LF_0C_2$  and  $LF_{0.15}C_2$  samples became rougher and had an uneven, porous structure due to the formation of a composite gel between curdlan and LMA-AM-AA polymer.

### 3.3 Performance comparison

#### (1) Comparison of the self-healing time

The self-healing time of the different samples in bentonite mud was investigated, and the gel pictures after self-healing are shown in Fig. 5. All sample particles were successfully self-healed into a whole gel after swelling in bentonite mud, indicating that the self-healing process could be achieved due to the hydrophobic association, ionic bonds and hydrogen bonds. However, the self-healing times of the different samples varied, as shown in Fig. 6. The  $LF_0C_0$  sample completed self-healing after 4.5 h, but under the same conditions, the  $LF_{0.15}C_0$  sample completed self-healing after only 3 h. Similarly, the self-healing time of  $LF_{0.15}C_2$  was 7 h, which was significantly lower than that of  $LF_0C_2$  sample (13 h). The self-healing times of  $LF_{0.05}C_2$  and  $LF_{0.25}C_2$  were 9 h and 5.5 h, respectively. These results showed that the introduction of  $Fe^{3+}$  in the polymer network of the gel could shorten the self-healing ti-

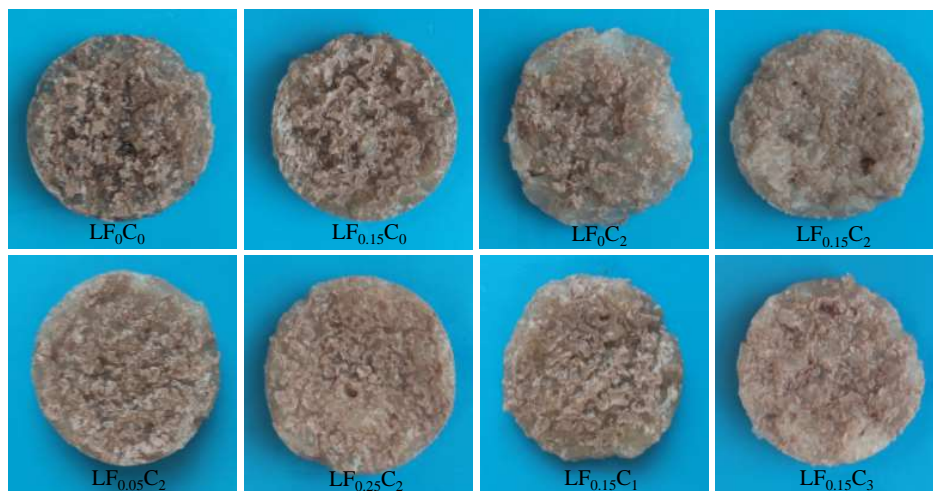


**Fig. 5.** Pictures of the different samples after self-healing.

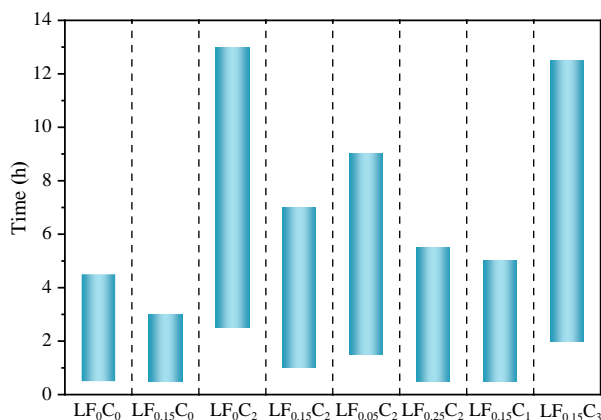


**Fig. 6.** Self-healing time of the different samples.

me of the sample, and with increasing  $\text{Fe}^{3+}$  concentration, the self-healing time of the sample was shortened. This was mainly due to the coordination between the carboxyl group on the gel molecular chain and the free  $\text{Fe}^{3+}$ , which accelerated the self-healing process and shortened the self-healing time (Qin et al., 2018; Zeng et al., 2022). By comparing the self-healing time of LF<sub>0</sub>C<sub>0</sub> and LF<sub>0</sub>C<sub>2</sub> samples, the self-healing time of the sample was significantly extended from 4.5 h to 13 h after adding curdlan. By comparing the self-healing times of the LF<sub>0.15</sub>C<sub>1</sub>, LF<sub>0.15</sub>C<sub>2</sub> and LF<sub>0.15</sub>C<sub>3</sub> samples, the greater amount of curdlan added correlated to a longer self-healing time because curdlan formed an irreversible gel with certain rigidity at high temperature; this irreversible gel formation hindered the diffusion of free LMA and SDS, and the mobility of the molecular chain was weakened. Thus, the reorganization of the hydrophobic association region was slowed down and the coordination efficiency of carboxyl groups with metal ions was reduced (Ye et al., 2020).

#### (2) Comparison of mechanical properties

Mechanical properties are also important indicators for evaluating gel plugging materials. Therefore, the mechanical properties of the self-healing gel were evaluated via tensile and compression experiments (Figs. 7 and S4). LF<sub>0</sub>C<sub>0</sub> sample

showed a relatively low elastic modulus (0.81 kPa) and poor toughness ( $5.2 \text{ kJ/m}^3$ ) after self-healing. The elastic modulus and toughness of LF<sub>0.15</sub>C<sub>0</sub> self-healing gel after adding  $\text{Fe}^{3+}$  were significantly improved to 1.69 kPa and  $15.1 \text{ kJ/m}^3$ , respectively. Additionally, the elastic modulus and toughness of LF<sub>0.15</sub>C<sub>2</sub> self-healing gel were also significantly better than those of LF<sub>0</sub>C<sub>2</sub>. This improvement was mainly attributed to the coordination bond between carboxyl group and  $\text{Fe}^{3+}$  on the polymer molecular chain, which increased the cross-linking points inside the gel network, resulting in a stronger network structure of the gel (Zeng et al., 2022). Thus, it significantly improved the overall mechanical properties of the gel, which was consistent with the SEM characterization results. However, from the experimental results of Fig. 7(b), with increasing of  $\text{Fe}^{3+}$  concentration, the mechanical properties of the self-healing gel initially increased and then decreased. Compared with LF<sub>0.15</sub>C<sub>2</sub> self-healing gel, the fracture stress of the LF<sub>0.25</sub>C<sub>2</sub> decreased from 8.58 kPa to 7.78 kPa when the addition of  $\text{Fe}^{3+}$  increased to 0.25 g, and the elastic modulus and toughness decreased to 2.96 kPa and  $22.8 \text{ kJ/m}^3$ , respectively. This phenomenon occurred because excessive  $\text{Fe}^{3+}$  caused the pH of the system to decrease; thus, the cross-linking was not uniform, resulting in low stability constant (Li et al., 2018). By comparing the self-healing gels of LF<sub>0.15</sub>C<sub>0</sub>, LF<sub>0.15</sub>C<sub>2</sub> and LF<sub>0</sub>C<sub>0</sub>, LF<sub>0</sub>C<sub>2</sub>, the elastic modulus and toughness of the self-healing gel were significantly improved after the introduction of curdlan. This occurred because curdlan and the polymer LMA-AM-AA network formed a composite network structure and improved the mechanical properties (Ye et al., 2020). The elastic modulus and toughness of LF<sub>0.15</sub>C<sub>2</sub> self-healing gel were 3.51 kPa and  $30.2 \text{ kJ/m}^3$ , respectively. Upon further increasing the amount of curdlan, the elastic modulus of LF<sub>0.15</sub>C<sub>3</sub> reached 4.94 kPa, but the toughness slightly decreased ( $21.9 \text{ kJ/m}^3$ ). This potentially occurred because the excessive curdlan increased the rigidity of the gel and negatively affected the toughness (Li et al., 2018; Zheng et al., 2020).

Moreover, the compression performance of the sample is also a key factor in evaluating the gel plugging material. From

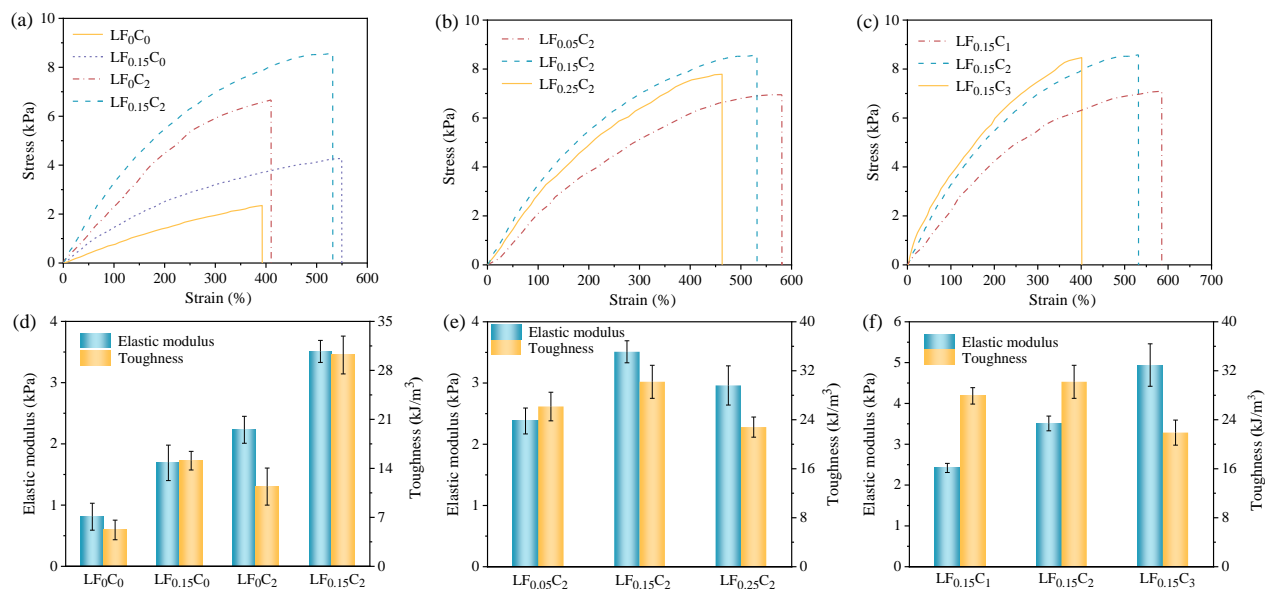


**Fig. 7.** (a)~(c) Tensile stress–strain curves of different samples, (d)~(f) Elastic modulus and toughness of different samples.

Fig. S4(a), the compression performance of the gel after the introduction of  $\text{Fe}^{3+}$  was significantly improved. From Fig. S4(b), with increasing  $\text{Fe}^{3+}$  content, the compression strength of the gel initially increased and then decreased, which was consistent with the trend of the tensile results. The compressive properties of the self-healing gels gradually increased with increasing curdlan concentration (Fig. S4(c)). Because curdlan formed a composite network structure with P(LMA-AM-AA) (Ye et al., 2020).

### (3) Comparison of rheological properties

The rheology of self-healing gel is predominantly used to study the dynamic viscoelastic properties of gel under shear action, which is the key index of the LCM; the storage modulus ( $G'$ ) is an important parameter to characterize the rheological properties of gel in fractures. Figs. 8(a)~8(c) shows the strain scanning curve of the self-healing gels from 0% to 1000%. Outside the linear viscoelastic region,  $G'$  decreases significantly with increasing strain, indicating that the physical noncovalent bond crosslinking in the gel network gradually dissociates. However, the  $G'$  value of the gel is always much larger than the corresponding  $G''$  values, indicating that the hydrogel mainly has the elastic solid properties (Bai et al., 2022). Fig. 8(d) shows that the  $G'$  values of the LF<sub>0</sub>C<sub>0</sub> and LF<sub>0</sub>C<sub>2</sub> self-healing gels are 1,519 Pa and 2,894 Pa, and the  $G''$  values are 293 Pa and 523 Pa, respectively. Additionally, the  $G'$  values of the LF<sub>0.15</sub>C<sub>0</sub> and LF<sub>0.15</sub>C<sub>2</sub> self-healing gels are 2,105 Pa and 3,458 Pa, and the  $G''$  values are 383 Pa and 594 Pa, respectively. This indicates that after addition of  $\text{Fe}^{3+}$ , the samples exhibit a relatively high storage modulus, which is mainly attributed to the coordination between  $\text{Fe}^{3+}$  and gel network molecules (Zheng et al., 2020). With increasing  $\text{Fe}^{3+}$  content, the interaction and storage modulus gradually increase. However, the excess  $\text{Fe}^{3+}$  changes the coordination environment of the system and limits the movement of the molecular chain; thus, the storage modulus of LF<sub>0.25</sub>C<sub>2</sub> de-

creases (Fig. 8(e)), which is consistent with the tensile test results.

Moreover, the  $G'$  of LF<sub>0.15</sub>C<sub>2</sub> was significantly higher than that of LF<sub>0.15</sub>C<sub>0</sub>, and the  $G'$  of LF<sub>0.15</sub>C<sub>1</sub>, LF<sub>0.15</sub>C<sub>2</sub> and LF<sub>0.15</sub>C<sub>3</sub> showed a gradual increasing trend (Fig. 8(f)), which indicated that the introduction of curdlan could effectively improve the storage modulus of the self-healing gels. Figs. 8(g)~8(i) shows the frequency scanning test results of different samples in the range from 0.1 to 100 rad/s. In the whole frequency scanning range, the  $G'$  values of all samples were always higher than  $G''$  values, and  $G'$  of the gel increased with increasing frequency. The modulus had a certain dependence on the frequency, and the gel maintained its elastic solid properties. This was due to the difficulty of immediate rearrangement of macromolecular chains in the gel sample as the frequency increased and the hardening of the gel (Bai et al., 2022).

The loss factor values ( $\tan\delta = G''/G'$ ) of the self-healing gel were calculated, and the results are shown in Fig. S5. The  $\tan\delta$  values of all samples were less than 1, indicating that the samples were elastic (Gulyuz and Okay, 2015). The elasticity of the sample increased with decreasing  $\tan\delta$  value. The  $\tan\delta$  of LF<sub>0.15</sub>C<sub>2</sub> was in the range of 0.8 to 1, indicating that it had good elastic recovery performance. Although LF<sub>0.15</sub>C<sub>3</sub> showed higher  $G'$ , its  $\tan\delta$  was higher than that of LF<sub>0.15</sub>C<sub>2</sub>. This was potentially because excessive curdlan increased the rigidity of the gel, hindered the movement of the molecular chain and affected the recovery performance (Ye et al., 2020; Bai et al., 2022).

Therefore, through the comprehensive comparison of the self-healing time, mechanical properties and rheological properties of different samples, subsequent further evaluation was carried out with the LF<sub>0.15</sub>C<sub>2</sub> sample as an example. Fig. 9(a) shows the intuitive self-healing pictures of LF<sub>0.15</sub>C<sub>2</sub> gel particles in bentonite mud and bentonite mud with rhodamine

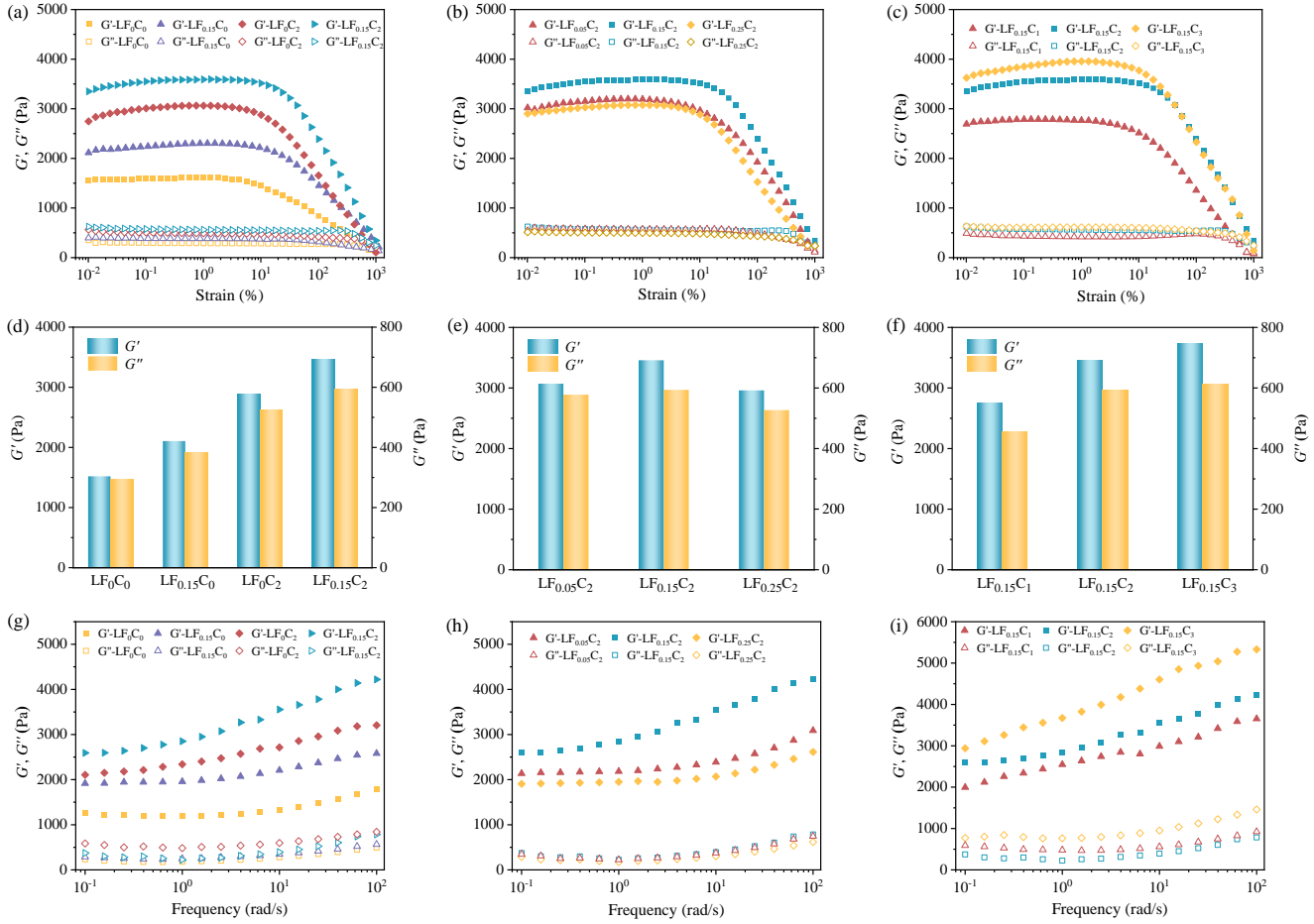


**Fig. 8.** (a)~(c) Dynamic strain sweep of different samples, (d)~(f)  $G'$  and  $G''$  of different samples., (g)~(i) dynamic frequency sweep of different samples.

B. The two colour gels self-healed from multiple independent states to a whole gel, and the self-healing gel had apparent toughness (Fig. 9(b)). To further verify the self-healing properties of the LF<sub>0.15</sub>C<sub>2</sub> samples, the step-strain ( $\gamma_{\min} = 1\%$ ,  $\gamma_{\max} = 1100\%$ ,  $\omega = 6.28$  rad/s) of LF<sub>0.15</sub>C<sub>2</sub> self-healing gel was evaluated (Fig. 9(c)). Under the condition of 1% strain,  $G' > G''$ , which was a stable gel structure. When the strain mutation was 1100%,  $G' < G''$ , indicating that the structure of the gel was destroyed and the gel was in the sol state. When the strain was changed to 1%,  $G' > G''$ , indicating that the self-healing gel was restored to gel. This phenomenon was mainly attributed to the dynamic balance between the polymer chain movement and the physical crosslinking point. This again confirmed that the gel had an effective self-healing ability. The LF<sub>0.15</sub>C<sub>2</sub> self-healing gel was scanned at  $\gamma = 1\%$  and  $\omega = 6.28$  rad/s, and the results are shown in Fig. 9(d). The values of  $G'$  and  $G''$  did not decrease significantly throughout the scan range, indicating that the self-healing gel had good stability.

### 3.4 Effect of particle size on self-healing gel properties

Particle size is an important investigation component of the self-healing gel applied to plugging. The pictures of the LF<sub>0.15</sub>C<sub>2</sub> gel particles with different particle sizes after self-healing are shown in Fig. 10(a). Gel particles with particle sizes of 0.2~1 mm, 1~3 mm and 3~5 mm could achieve self-healing in the bentonite mud. Besides, the  $G'$  value of the gel after self-healing increased with increasing particle size (Fig. 10(c)). However, as the particle size increased, the self-healing time of the sample was gradually extended. The reason for this phenomenon was that as the particle size increased, the contact area between the expanded gel decreased; thus, the self-healing time was extended.

### 3.5 Effect of salt on self-healing gel properties

During drilling, high-salinity formations are often encountered. Therefore, the effect of salt on the properties of self-healing gels needs to be examined. Fig. 11 shows the self-healing of self-healing gel particles in bentonite mud, 5%

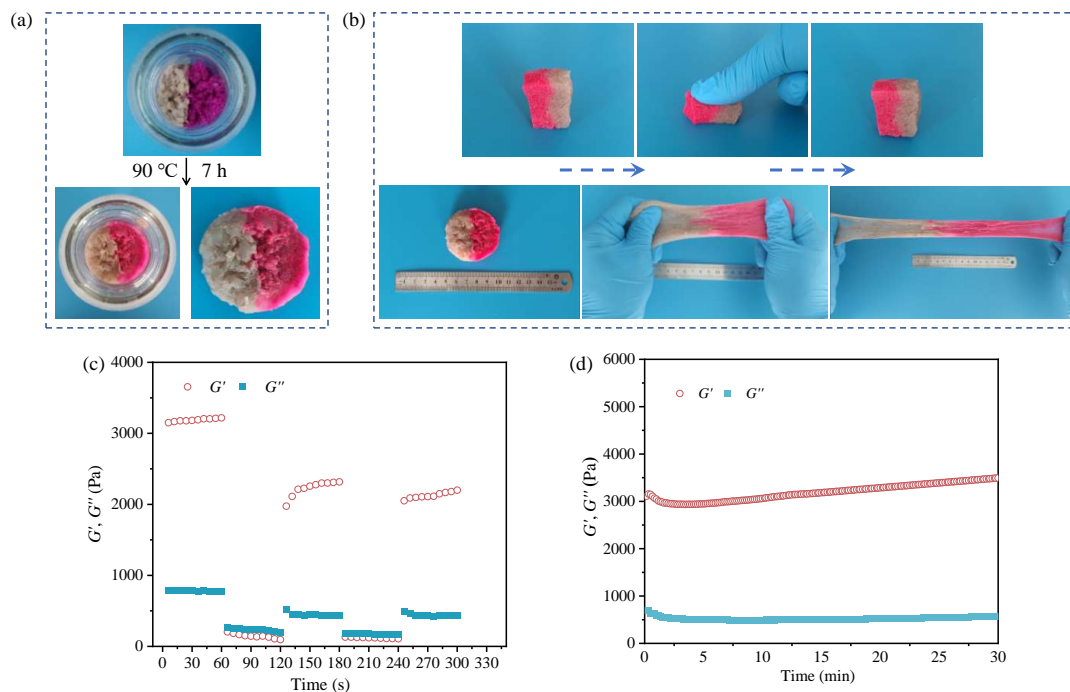


**Fig. 9.** (a) Physical pictures of  $LF_{0.15}C_2$  gel before and after healing, (b) stretching and compression pictures of self-healing gel, (c) step-strain test of  $LF_{0.15}C_2$  gel and (d) time sweep of  $LF_{0.15}C_2$  gel.

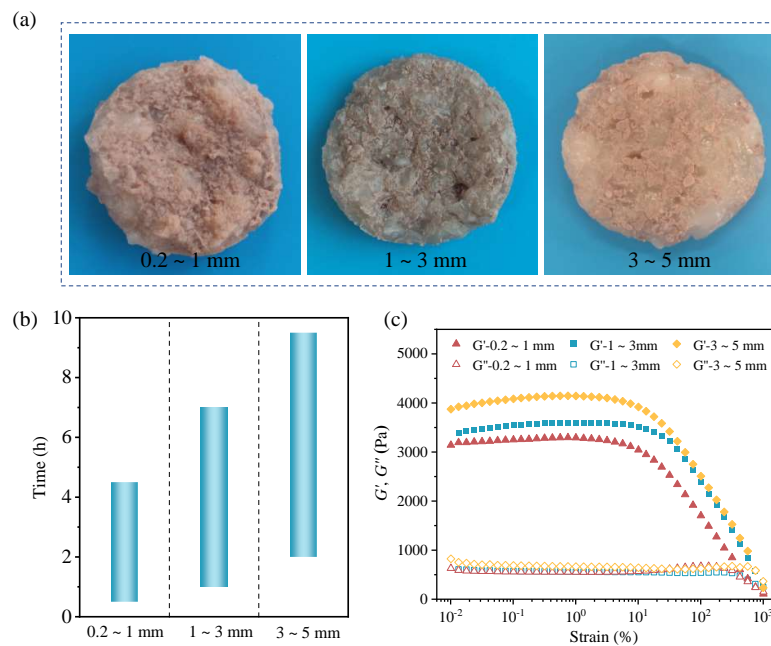


**Fig. 10.** Performance evaluation of  $LF_{0.15}C_2$  particles with different particle sizes. (a) Pictures after self-healing in mud, (b) self-healing time evaluation and (c) dynamic strain sweep.

NaCl-mud, 10% NaCl-mud and 2%  $CaCl_2$ -mud. The self-healing gel particles could self-heal as a whole in different concentrations of NaCl and  $CaCl_2$  (Fig. 11(a)), and from Fig. 11(b), different concentrations of NaCl and  $CaCl_2$  had negligible effect on the self-healing time of the gel. The rheological strength of  $LF_{0.15}C_2$  sample after self-healing in

different concentrations of NaCl and  $CaCl_2$  was tested, and the results are shown in Fig. 11(c). Compared with the self-healing gel in mud, the  $G'$  of the self-healing gel in 5% NaCl-mud increased due to the formation of more hydrophobic microdomains in the NaCl-induced gel molecular network and the enhancement of hydrophobic association (Zhang et al.,

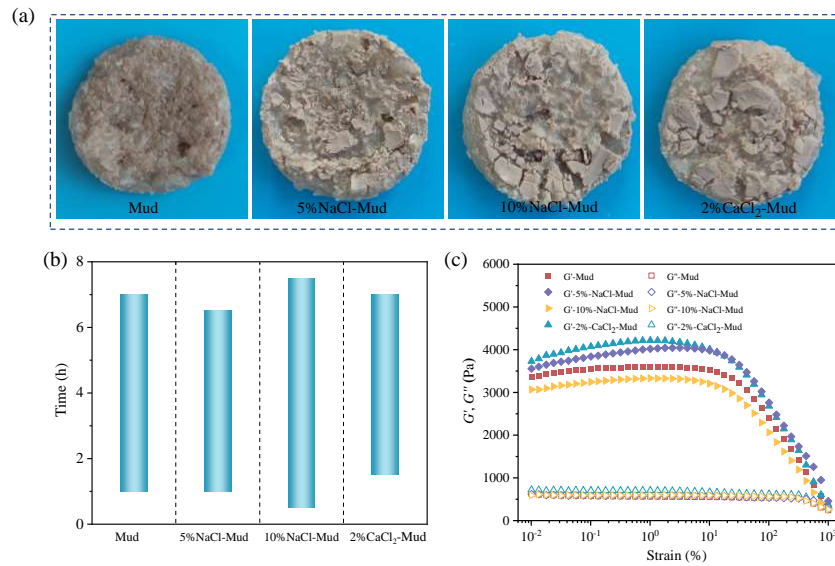


**Fig. 11.** Performance evaluation of the LF<sub>0.15</sub>C<sub>2</sub> with salt solutions. (a) Pictures after self-healing in mud, (b) self-healing time evaluation and (c) dynamic strain sweep.

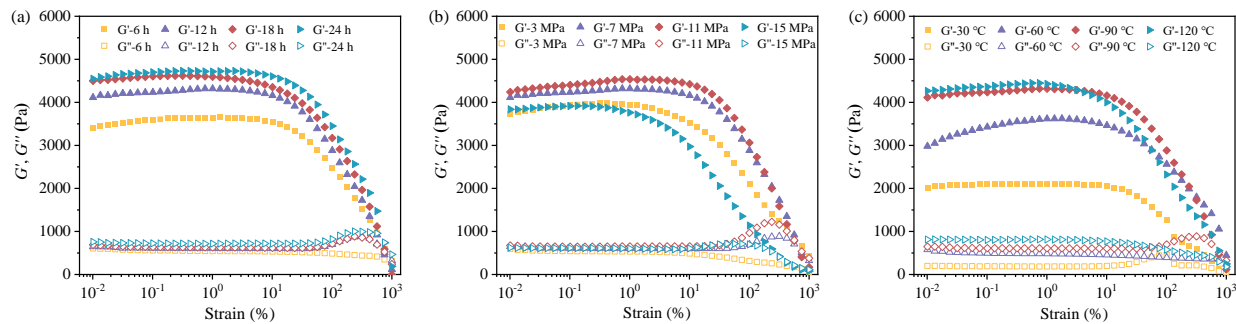


**Fig. 12.** Strain sweep curves of self-healing gel under different reaction conditions (a) Different reaction times, (b) different reaction pressures and (c) different reaction temperatures.

2020). However, the rheological strength  $G'$  of the gel after self-healing in 10% NaCl-mud slightly decreased due to the ion effect. Excessive sodium chloride affected the coordination of iron and carboxyl groups, and the electrostatic interaction was weakened (Zhang et al., 2018). Moreover, the  $G'$  of the gel after self-healing in 2% CaCl<sub>2</sub>-mud was also increased due to the coordination structure formed by Ca<sup>2+</sup> and carboxyl groups in the molecular network. These results indicated that the LF<sub>0.15</sub>C<sub>2</sub> sample could still maintain a certain rheological strength in salt solution and had salt resistance (Yu et al., 2022).

### 3.6 Effect of reaction time, pressure and temperature on self-healing gel properties

Reaction time is an important factor affecting the performance of self-healing gels in fractures; thus, the effect of different reaction times on the rheological strength of self-healing gels was investigated. Fig. 12(a) shows rheological curves of self-healing gels after different reaction times (reaction temperature and pressure are 90 °C and 7 MPa, respectively).

As the reaction time increased, the  $G'$  of the self-healing gel gradually increased. This occurred because the degree of self-healing increased with the extension of self-healing time (Ye et al., 2020). However, the  $G'$  of the gel did not change significantly after reaction times of 18 and 24 h, indicating that the degree of self-healing had reached the threshold at this time. Continuing to increase the self-healing time did not significantly increase the  $G'$  value of the gel.

The reaction pressure is an important downhole environmental factor. The rheological properties of self-healing gels at different pressures (3, 7, 11 and 15 MPa) were investigated. The results are shown in Fig. 12(b). When the reaction temperature was 90 °C and the reaction time was 12 h, the  $G'$  values of the self-healing gel after reaction at 7 MPa and 11 MPa were 4,219 Pa and 4,503 Pa, respectively, which were significantly higher than those at 3 MPa (3,857 Pa). However, when the reaction pressure was higher than 15 MPa, the  $G'$  of the sample showed a downwards trend. This indicated that increasing the pressure conditions of the reaction promoted the contact between the interfaces between relatively independent

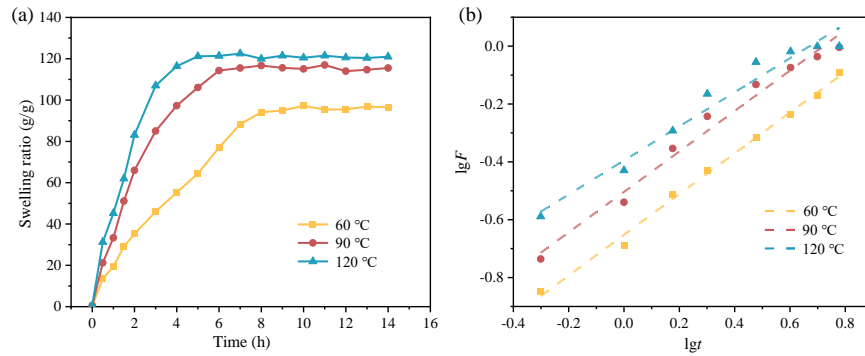


**Fig. 13.** (a) Swelling behavior of LF<sub>0.15</sub>C<sub>2</sub> sample and (b) swelling kinetics of LF<sub>0.15</sub>C<sub>2</sub> sample.

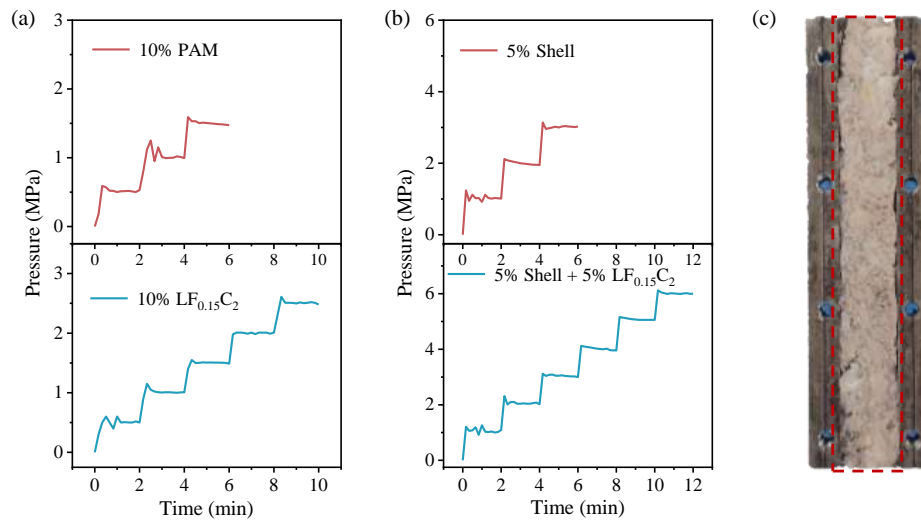


**Fig. 14.** (a)~(b) Pressure-bearing plugging performance using LCM, (c) the pictures of self-healing gel in fractured metal core.

gels, thereby increasing the migration of molecular chains between the interfaces. However, excessive pressure caused the molecular chains in the gel structure to break, leading to a decrease in the storage modulus of the gel after self-healing.

The reaction temperature is a key and important external factor affecting the performance of the self-healing gel. Therefore, rheological curves of the sample at different temperatures (30, 60, 90 and 120 °C) are shown in Fig. 12(c). At a pressure of 7 MPa and a reaction time of 12 h, the  $G'$  value gradually increased with increasing temperature. The reason for this phenomenon was that as the temperature increased, the solubility of the hydrophobic part of the hydrophobically associating gel sample in the aqueous solution increased, and the mobility of the molecular chain increased; thus, that the polymer chains on the surface of the mutually independent gel could more easily diffuse from one side to the other side. Moreover, the rheological properties of the self-healing gel modified by curdlan were enhanced under high temperature (Ye et al., 2020).

To further illustrate the effect of temperature, the swelling behaviour of LF<sub>0.15</sub>C<sub>2</sub> sample at different temperatures was investigated. Fig. 13(a) shows the swelling curve of the

LF<sub>0.15</sub>C<sub>2</sub> particles in bentonite mud. With increasing time, the swelling rate of the LF<sub>0.15</sub>C<sub>2</sub> particles in bentonite mud gradually increased and finally reached equilibrium. Moreover, the equilibrium swelling ratios of the LF<sub>0.15</sub>C<sub>2</sub> particles at 60, 90 and 120 °C were 95.4, 115.1 and 121.9 g/g, respectively, indicating that the samples had excellent swelling properties. With increasing temperature, the equilibrium swelling ratio of the LF<sub>0.15</sub>C<sub>2</sub> particles in bentonite mud gradually increased and the time to reach the equilibrium swelling ratio was gradually shortened. To further explore the swelling behaviour of the LF<sub>0.15</sub>C<sub>2</sub> particles, the swelling rate at the initial stage of swelling (0.5~6 h) was fitted by the Fickian diffusion model (Wei et al., 2013). The Fickian diffusion model can be described by Eqs. (2) and (3), and the fitting results are shown in Fig. 13(b) and Table 2. All curves had a good linear relationship, indicating that the Fickian diffusion model was suitable for evaluating the initial swelling of the LF<sub>0.15</sub>C<sub>2</sub> gel at different temperatures. The diffusion index  $n$  values at 60, 90 and 120 °C were 0.704, 0.699 and 0.589, respectively; these were in the range of 0.5~1, indicating that the swelling stage of the LF<sub>0.15</sub>C<sub>2</sub> sample was non-Fickian diffusion, and the absorption of water was controlled by the diffusion of water

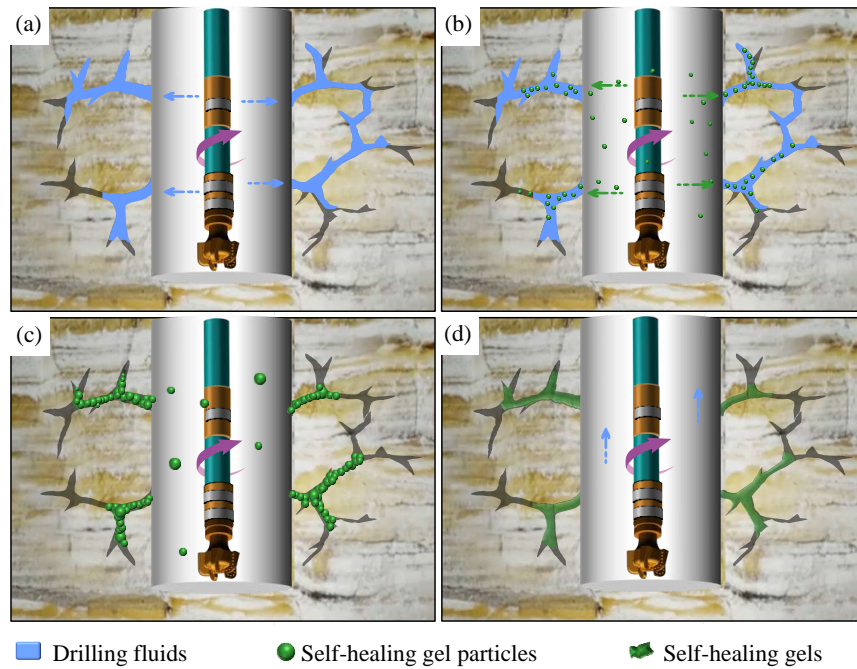


**Fig. 15.** Plugging mechanism of self-healing gel particles.

**Table 2.** Swelling kinetic parameters of LF<sub>0.15</sub>C<sub>2</sub> sample.

Temperature (°C)	$n$	Intercept	$R^2$
60	0.704	-0.652	0.9952
90	0.699	-0.503	0.9813
120	0.589	-0.395	0.9638

and the relaxation of the polymer molecular chain (Wei et al., 2013):

$$F = \frac{w_t}{w_e} = Kt^n \quad (2)$$

$$\lg F = \lg K + n \lg t \quad (3)$$

where  $F$  is the percentage of water absorption at time  $t$ ,  $w_t$ (g) and  $w_e$ (g) are the water absorption at time  $t$  and equilibrium, respectively,  $K$  is the ratio constant of the gel, and  $n$  is the Fickian diffusion index.

### 3.7 Test of plugging performance

The plugging performance is a key indicator for evaluating LCM; thus, the pressure-bearing performance of the sample in the metal slit plate is studied (Fig. 14). The plugging performance of the LF<sub>0.15</sub>C<sub>2</sub> sample is 2.5 MPa, which is significantly higher than that of conventional gel PAM (1.5 MPa). This is mainly because LF<sub>0.15</sub>C<sub>2</sub> self-healing gel can self-heal into a whole gel in fractures at high temperature (Fig. 14(c)), which can effectively fill and plug entire fracture, improve the mechanical properties of the LCM. From the comparison of the pressure-bearing properties of 10% shell and 5% shell+5% LF<sub>0.15</sub>C<sub>2</sub>, the pressure-bearing capacity of 10% shell is 3 MPa, and the pressure-bearing performance

is improved to 6 MPa by compounding 5% shell and 5% LF<sub>0.15</sub>C<sub>2</sub>. From the picture of fractured metal core, the 10% shell easily causes plugging at the entrance of the fractures (Fig. S6), while 5% shell+5% LF<sub>0.15</sub>C<sub>2</sub> does not exhibit this phenomenon. The reason for this phenomenon is that the matching between the shell and the fracture is poor. By reducing the concentration of the shell and adding the self-healing gel with deformability, the shell and the gel can enter the fracture to achieve the effect of effectively filling and plugging the fracture, thus improving the pressure-bearing performance. In general, due to their self-healing properties and deformability, self-healing gels have application prospects in the field of plugging.

Based on deformability and self-healing properties of the self-healing gel, the plugging mechanism of the self-healing gel in formation fractures was deduced. In the process of downhole operation, the working fluid flowed into the formation fracture under the action of pressure difference, resulting in the leakage of working fluid (Fig. 15(a)). The self-healing gel particles could enter the wellbore with the working fluid and enter the fracture under the pressure difference between the drilling fluid column and the formation pressure (Fig. 15(b)). The particles entering the fractures gradually absorbed water and swelled, resulting in a gradual increase in volume and becoming a gel with deformability and self-healing properties (Fig. 15(c)) (Bai et al., 2022). With the gradual increase and expansion of the gel in the fracture, independent gel extrusion and aggregation occurred. Moreover, under the action of the formation temperature, the diffusion of molecular chains and Fe<sup>3+</sup> gradually occurred between the independent but contact interfaces, and the free LMA fragments were redissolved in SDS micelles. The six-fold triple helix in the gel

polysaccharide increased due to the high temperature produced (Ye et al., 2020). With the extension of time, the hydrophobic association and ionic bond between independent gels were reformed and then became a whole gel to fill and plug fractures (Fig. 15(d)).

#### 4. Conclusions

In summary, self-healing gels modified with curdlan and  $\text{Fe}^{3+}$  were successfully synthesized by a facile method. The mechanical properties and rheological properties of the self-healing gels could be effectively improved by the modification of curdlan and the introduction of  $\text{Fe}^{3+}$  in a certain range. The  $\text{LF}_{0.15}\text{C}_2$  self-healing gel had good performance, and its elastic modulus and toughness were 3.51 kPa and 30.2  $\text{kJ/m}^3$ , respectively. The  $G'$  was 3,458 Pa, and the self-healing time at 90 °C was 7 h. Moreover, increasing the temperature, pressure and time of the self-healing reaction could increase the  $G'$  value of self-healing gel. The self-healing gel was applied to the plugging of formation fractures in oil and gas drilling. The pressure-bearing experiment showed that the pressure-bearing performance of  $\text{LF}_{0.15}\text{C}_2$  self-healing gel was 2.5 MPa, which was better than the 1.5 MPa pressure-bearing capacity of conventional gel PAM. Moreover, the pressure bearing capacity of the self-healing gel combined with the shell could reach 6 MPa. Therefore, the self-healing gel modified by curdlan could be a promising LCM.

#### Acknowledgements

This work was supported by the National Natural Science Foundation of China (No. 52174016), the CNPC's Major Science and Technology Project (Nos. 2021DJ4404 and 2021DJ6601), the Scientific Research and Technology Development Project of CNPC Engineering Technology R&D Company Limited (No. CPET2022-06S).

#### Supplementary file

<https://doi.org/10.46690/ager.2023.05.05>

#### Conflict of interest

The authors declare no competing interest.

**Open Access** This article is distributed under the terms and conditions of the Creative Commons Attribution (CC BY-NC-ND) license, which permits unrestricted use, distribution, and reproduction in any medium, provided the original work is properly cited.

#### References

- Abbas, A. K., Bashikh, A. A., Abbas, H., et al. Intelligent decisions to stop or mitigate lost circulation based on machine learning. *Energy*, 2019, 183: 1104-1113.
- Ahdaya, M., Al Brahim, A., Bai, B. J., et al. Low-temperature recrosslinkable preformed particle gel as a material for lost circulation control. *SPE Journal*, 2022, 27(5): 2541-2551.
- Alhaidari, S. A., Alarifi, S. A., Bahamdan, A. Plugging efficiency of flaky and fibrous lost circulation materials in different carrier fluid systems. *Frontiers in Physics*, 2022, 10: 1065526.
- Al-Ibadi, A., Civan, F. Experimental investigation and correlation of treatment in weak and high-permeability formations by use of gel particles. *SPE Production & Operations*, 2013, 28(4): 387-401.
- Alkinani, H. H., Al-Hameedi, A. T. T., Dunn-Norman, S., et al. Using data mining to stop or mitigate lost circulation. *Journal of Petroleum Science and Engineering*, 2019, 173: 1097-1108.
- Aquinas, N., Bhat, M. R., Selvaraj, S. A review presenting production, characterization, and applications of biopolymer curdlan in food and pharmaceutical sectors. *Polymer Bulletin*, 2022, 79(9): 6905-6927.
- Bai, Y., Zhang, Q., Sun, J., et al. Double network self-healing hydrogel based on hydrophobic association and ionic bond for formation plugging. *Petroleum Science*, 2022, 19(5): 2150-2164.
- Christopher, J. E. P., Sultan, M. T. H., Selvan, C. P., et al. Manufacturing challenges in self-healing technology for polymer composites-a review. *Journal of Materials Research and Technology*, 2020, 9(4): 7370-7379.
- Davydovich, D., Urban, M. W. Water accelerated self-healing of hydrophobic copolymers. *Nature Communications*, 2020, 11(1): 5743.
- Feldner, T., Haring, M., Saha, S., et al. Supramolecular metallohydrogel that imparts self-healing properties to other gel networks. *Chemistry of Materials*, 2016, 28(9): 3210-3217.
- Gulyuz, U., Okay, O. Self-healing poly (N-isopropylacrylamide) hydrogels. *European Polymer Journal*, 2015, 72: 12-22.
- Hino, T., Ishimoto, H., Shimabayashi, S. Thermal gelation of aqueous curdlan suspension: preparation of curdlan jelly. *The Journal of Pharmacy and Pharmacology*, 2003, 55(4): 435-441.
- Hsieh, W. C., Hsu, C. C., Shiu, L. Y., et al. Biocompatible testing and physical properties of curdlan-grafted poly (vinyl alcohol) scaffold for bone tissue engineering. *Carbohydrate Polymers*, 2017, 157: 1341-1348.
- Hussain, I., Sayed, S. M., Liu, S. L., et al. Hydroxyethyl cellulose-based self-healing hydrogels with enhanced mechanical properties via metal-ligand bond interactions. *European Polymer Journal*, 2018, 100: 219-227.
- Li, X., Wang, H., Li, D., et al. Dual ionically cross-linked double-network hydrogels with high strength, toughness, swelling resistance, and improved 3D printing processability. *ACS Applied Materials & Interfaces*, 2018, 10(37): 31198-31207.
- Lian, P., Li, L., Duan, T. Injection parameters optimization of crosslinked polymer flooding by genetic algorithm. *Advances in Geo-Energy Research*, 2018, 2(4): 441-449.
- Mansour, A., Taleghani, A. D., Salehi, S., et al. Smart lost circulation materials for productive zones. *Journal of Petroleum Exploration and Production Technology*, 2019, 9(1): 281-296.
- Marubayashi, H., Yukinaka, K., Enomoto-Rogers, Y., et al. Curdlan ester derivatives: Synthesis, structure, and properties. *Carbohydrate Polymers*, 2014, 103: 427-433.
- Michael, F. M., Krishnan, M. R., AlSoughayer, S., et

- al. Thermo-elastic and self-healing polyacrylamide-2D nanofiller composite hydrogels for water shutoff treatment. *Journal of Petroleum Science and Engineering*, 2020, 193: 107391.
- Pandya, K. S., Naik, N. K. Nanoparticle dispersed resins and composites under quasi-static loading: Shear plugging behavior. *Polymer Composites*, 2016, 37(12): 3411-3415.
- Qin, Z., Niu, R., Tang, C., et al. A dual-crosslinked strategy to construct physical hydrogels with high strength, toughness, good mechanical recoverability, and shape-memory ability. *Macromolecular Materials and Engineering*, 2018, 303(2): 1700396.
- Schuman, T., Salunkhe, B., Al Brahim, A., et al. Evaluation of ultrahigh-temperature-resistant preformed particle gels for conformance control in north sea reservoirs. *SPE Journal*, 2022, 27(6): 3660-3673.
- Tang, M., Wang, C., Deng, X., et al. Experimental investigation on plugging performance of nanospheres in low-permeability reservoir with bottom water. *Advances in Geo-Energy Research*, 2022, 6(2): 95-103.
- Taylor, D. L., Panhuis, M. I. H. Self-Healing hydrogels. *Advanced Materials*, 2016, 28(41): 9060-9093.
- Tuncaboylu, D. C., Sari, M., Oppermann, W., et al. Tough and self-healing hydrogels formed via hydrophobic interactions. *Macromolecules*, 2011, 44(12): 4997-5005.
- Wang, C., Sun, J., Long, Y., et al. A re-crosslinkable composite gel based on curdlan for lost circulation control. *Journal of Molecular Liquids*, 2023, 371: 121010.
- Wei, Q., Luo, Y., Fu, F., et al. Synthesis, characterization, and swelling kinetics of pH-responsive and temperature-responsive carboxymethyl chitosan/polyacrylamide hydrogels. *Journal of Applied Polymer Science*, 2013, 129(2): 806-814.
- Ye, L., Lv, Q., Sun, X., et al. Fully physically cross-linked double network hydrogels with strong mechanical properties, good recovery and self-healing properties. *Soft Matter*, 2020, 16(7): 1840-1849.
- Yu, B., Zhao, S., Long, Y., et al. Comprehensive evaluation of a high-temperature resistant re-crosslinkable preformed particle gel for water management. *Fuel*, 2022, 309: 122086.
- Zeng, R., Qi, C., Lu, S., et al. Hydrophobic association and ionic coordination dual crossed-linked conductive hydrogels with self-adhesive and self-healing virtues for conformal strain sensors. *Journal of Polymer Science*, 2022, 60(5): 812-824.
- Zhang, B., Wang, C., Wang, Y., et al. A facile method to synthesize strong salt-enhanced hydrogels based on reversible physical interaction. *Soft Matter*, 2020, 16(3): 738-746.
- Zhang, R., Guo, J., Liu, Y., et al. Effects of sodium salt types on the intermolecular interaction of sodium alginate/antarctic krill protein composite fibers. *Carbohydrate Polymers*, 2018, 189: 72-78.
- Zhao, S., Al Brahim, A., Liu, J., et al. Coreflooding evaluation of fiber-assisted recrosslinkable preformed particle gel using an open fracture model. *SPE Journal*, 2023, 28(1): 268-278.
- Zhao, P., Qin, R., Pan, H., et al. Study on array laterolog response simulation and mud-filtrate invasion correction. *Advances in Geo-Energy Research*, 2019, 3(2): 175-186.
- Zheng, Q., Zhao, L., Wang, J., et al. High-strength and high-toughness sodium alginate/polyacrylamide double physically crosslinked network hydrogel with superior self-healing and self-recovery properties prepared by a one-pot method. *Colloids and Surfaces A: Physicochemical and Engineering Aspects*, 2020, 589: 124402.